Appl. Phys. B (2015) 119:551–557
DOI 10.1007/s00340-015-6042-z

Applied Physics B
Lasers and Optics

State-of-health meter fabricated using ultraviolet laser system for rapid evaluation of lithium-ion batteries

Min-Wei Hung · Kuo-Cheng Huang · Hsin-Yi Tsai · Chih-Chung Yang · Wen-Tse Hsiao · J. Andrew Yeh

Received: 22 September 2014 / Accepted: 4 February 2015 / Published online: 20 February 2015
© Springer-Verlag Berlin Heidelberg 2015

Abstract This study involved developing a meter for rapidly evaluating the state of health (SOH) of lithium-ion batteries (LIBs). The key component was a magnetic induction antenna (MIA) module with an interdigital pattern fabricated using a 355-nm pulsed ultraviolet laser system. For inducing high voltage from the LIB to the MIA module for evaluating the SOH, interdigital patterns of four line widths (i.e., 0.25, 0.5, 0.75, and 1.0 mm) were designed. The experimental results indicate that patterns with wider lines induce higher voltages. However, patterns using the 0.75-mm line offer optimal SOH measurements, because those with the 1.0-mm line yielded lower power storage. The optimal operating frequency for enhancing SOH identification was found to be 700 kHz. In addition, this study established an empirical equation for expressing the relationship between the induced voltage and SOH of LIBs.

1 Introduction

The lithium-ion battery (LIB) is widely used in portable electronic products and new energy technologies such as electric vehicles and electrical energy storage systems. The LIB has incomparable advantages over other rechargeable batteries, including a higher energy density, fewer maintenance requirements, a higher nominal voltage, and lower self-discharge rate; thus, the LIB is regarded as one of the most promising energy solutions. However, its performance deteriorates with time because of impacts from aging and its operating environment. Battery failure may result in serious, sometimes catastrophic, consequences. Therefore, it is desirable to estimate the state of health (SOH) of a battery to predict how soon it will fail or void the guarantee of satisfactory performance.

The aging of lithium (Li)-ion cells is a critical factor in all applications that employ this type of battery. Aging impacts battery performance [1] and, hence, modifies considerably the output parameters such as the SOH and state of charge (SOC). Electrochemical and electrical researchers use electrochemical impedance spectroscopy (EIS) measurements to examine aging. The EIS measurements provide electrochemical researchers with information about the kinetics in the electrodes (e.g., Li + diffusion rate) [2], information that assists the electrical researcher to ensure an accurate equivalent circuit of the battery. This common measurement technique has been studied for almost all battery chemistries, not only for the SOC but also for SOH determination [3, 4].

Typical methods of SOC estimation include ampere-hour counting (e.g., Coulomb counting), inverse nonlinear mapping from the open circuit voltage to the SOC, which includes the Kalman filter (KF) [5] and its extensions [6–8], methods based on artificial neural networks [9], and methods based on fuzzy logic [10]. Because the KF method cannot be used directly for the state prediction of a nonlinear system, methods based on the extended Kalman filter (EKF) [6, 7] and unscented Kalman filter (UKF) [11] are the most widely used. However, the EKF must compute the Jacobian matrix and is generally not suitable for highly nonlinear systems with non-Gaussian noise. Similarly, the

M.-W. Hung · K.-C. Huang (✉) · H.-Y. Tsai · C.-C. Yang · W.-T. Hsiao · J. Andrew Yeh
Instrument Technology Research Center, National Applied Research Laboratories, Hsinchu 30076, Taiwan
e-mail: huangkc@narlabs.org.tw

M.-W. Hung · J. Andrew Yeh
Institute of NanoEngineering and Microsystems, National Tsing Hua University, Hsinchu 30076, Taiwan

Table 1 Comparison of technology used in fabricating antennas for wireless microwave charging modules

Technology	Material	Fabricated type	Mask	Volume	Advantages and disadvantages
Coil	Wire	Additive	No	Large	1. Long fabricating time 2. Complex procedure (3–4 steps) 3. High induced power
Etching (FPC)	Thin film	Wet ablated	Yes	Small	1. Long fabricating time 2. Complex procedure (5–6 steps) 3. Flexible circuit pattern
Photo-excited (laser processing)	Thin film	Dry ablated	No	Small	1. Short processing time 2. Simple procedure (1 step) 3. High variability of pattern

UKF is another extension of the KF and is also a recursive minimum mean square error estimator. The UKF has been demonstrated to outperform the KF and EKF in terms of accuracy and robustness for nonlinear estimation. The UKF does not need to calculate the Jacobian matrix and does not require noise to be Gaussian, which makes it appealing for SOC estimation because battery systems are highly nonlinear and noise properties are typically not known.

The SOH of the battery reflects the decline of the battery capacity. For battery management, evaluating the SOH is critical [12, 13]. Hence, incremental capacity analysis (ICA) is used to analyze the SOH by differentiation of the voltage and capacity [12, 14], and a differential voltage analysis is used to analyze the battery charge–discharge data by employing the inverse data of the ICA [12, 15, 16]. Spotnitz et al. [17] used the capacity-fading model to determine the SOH of Li-ion cells; the model showed that the end of life (EOL) of the Li-ion cell is approximately 80 % of its nominal capacity. As shown by testing results [18], the EOL of an LIB occurs after 500 discharge and charge cycles. Commonly, the AC impedance spectrum is also employed to evaluate the SOH of the battery [19, 20]. In addition to these classic methods, the probability density function is another method for analyzing the condition of the battery [21].

Rechargeable LIBs are suitable candidates for implanted power sources because they have long cycle life, high energy density, and a favorable safety record. A primary battery is used as an implanted power source because there is no efficient way to charge the power source (i.e., a rechargeable battery). However, the measurement time of traditional methods for determining the SOH of LIBs is extremely long, and the measurement instrument is usually expensive and not suitable for general users to confirm the SOH of the LIB. To address these disadvantages and decide the performance and SOH of a battery rapidly, a micro-device was developed to detect signals induced by a wireless microwave charging module with a developed capacitor charged by LIBs. Generally, antennas used in wireless microwave charging modules have been fabricated using coils [22] and etching technology (i.e., flexible printed circuit, FPC) [23, 24], as shown in the summary comparing technology for fabricating antennas (Table 1). An antenna fabricated using coils and an etching method has several disadvantages such as long fabrication time, complex procedures, large volume, and the necessity of a pattern mask, reducing the variability of the antenna. When laser processing was employed to fabricate a magnetic antenna, the processing time and procedures saved were substantial, and the shape of the pattern could be adjusted readily. The laser beam was collected and focused onto a light spot in the laser system, which provided high energy and ablated the material coating the substrate. Hence, the laser processing method was classified as the photo-excited process. Yang et al. [25] demonstrated that a UV laser system can be used to fabricate the planar square-spiral inductances on a glass substrate for a wireless charging module, with a maximal value of 774 mV and an induction capacity of 11.34 % when the line width was 1.5 mm. In addition, Tsai et al. [26] determined that a magnetic field can be affected and induced by thermal stress when energy is exerted on the materials by a laser system, and the phase of the induced magnetic field increases with increasing ablation time and decreasing pattern angle.

In the study, we used a 355-nm UV laser system to create the interdigital pattern on the copper-coated glass substrate that served as a capacitor of the magnetic induction antenna (MIA). To obtain the optimal micromachining effect, MIAs with different line widths were designed and produced on the substrate surface by a laser direct-writing (LDW) technique. In addition, the MIA and the conversion circuit were integrated together and become a micro-device, called SOH meter, to measure the induced voltage and determine the SOH of the LIBs.

2 Experiment system and method

2.1 Experimental system

The LDW system consisted of a 355-nm diode-pumped solid-state Nd/YVO4 laser (Coherent, Inc.) employed

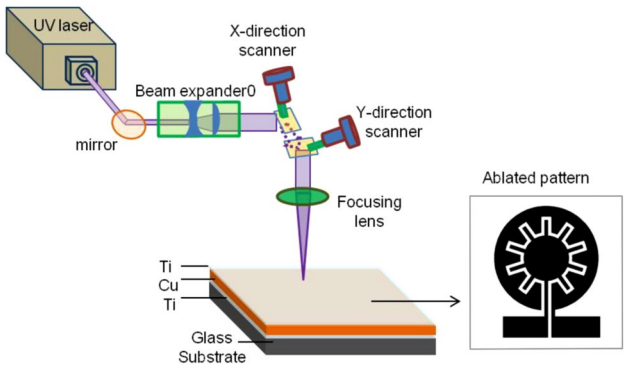

Fig. 1 Schematic of the laser ablation processing system

to ablate the materials coated on the glass substrate. The maximum power of the laser system was 14 W. The laser source output beam had a diameter of 3.5 mm, and the beam quality factor (i.e., M^2) was <1.3. The diameter of the laser beam was magnified by a 2× beam expander, with the direction of the laser beam transformed by three reflective mirrors. The laser was projected onto a high-speed galvanometer system composed of two mirrors with a set of focus shifters to adjust the focus position in a Z-direction with a range from −15 to 15 mm. The focal length of the telecentric focusing lens was 160 mm, and the spot size projected onto the working plane by the laser was approximately 13.5 μm. The power, pulse repetition rate, and scanning speed of the laser system affect the edge-aspect ratio, oxidation degree, and induction capacity of the ablated pattern [25]. The oxidation degree decreased and had a low value when the pulse repetition rate was set to 100 kHz; a low edge-aspect ratio (i.e., smooth pattern edge) and high induced voltage can be obtained simultaneously when the scanning speed was 500 mm/s. In addition, the substrate would rupture if the laser power was too high. Therefore, the laser power employed in the experiment was only 1 W; the pulse repetition frequency was fixed at 100 kHz, and the scanning speed was fixed at 500 mm/s. In addition, the scanning area used in the experiment was 30 × 30 mm^2. A schematic of the experimental system used for laser ablation processing is shown in Fig. 1.

2.2 Pattern design and sample preparation

In the study, the substrate was soda-lime glass, and its dimension was 30 × 30 × 0.5 mm^3. To determine the SOH of LIBs from signals induced by an MIA, a copper (Cu) material with a thickness of 200 nm was coated on the glass substrate because of its electrical conductivity. In addition, titanium (Ti) with a thickness of 20 nm was coated between the glass substrate and Cu layer and covered on the Cu layer to increase adhesion and avoid oxidation of the Cu layer, respectively. The composition of the material coated on the glass substrate is summarized in Table 2. The absorption of the coated materials was evaluated using the light reflectivity of the coated materials and Kirchhoff's law of thermal radiation. As shown in Fig. 2 by the spectrophotometer (HITACHI U3900), the coated material had lower reflectivity and higher absorption at 355 nm than at other wavelengths. Therefore, the laser source at a wavelength of 355 nm was employed in the photo-excited process. In addition, a smaller laser spot and sharper pattern edge could be obtained when the pattern was ablated by a 355-nm UV laser because the energy of the 355-nm UV laser was higher than that of a 532- or 1064-nm Nd/YAG laser.

Table 2 Composition of material-coated glass substrate

Layer	Material	Thickness
Substrate	Glass	500 μm
1	Ti	20 nm
2	Cu	200 nm
3	Ti	10 nm

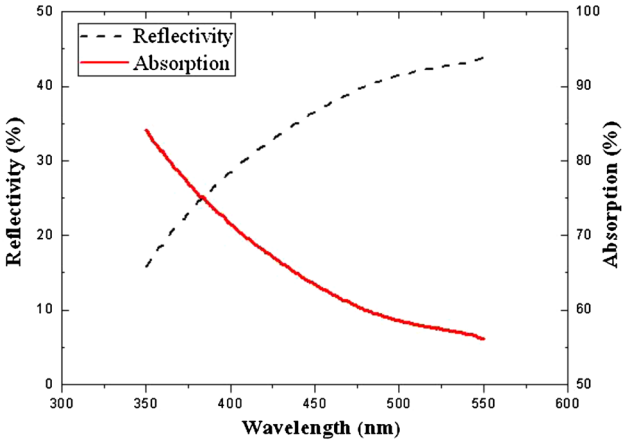

Fig. 2 Reflectivity and absorption of the coated material

In addition, the estimated capacitance value (C) between the two plates was calculated based on Gauss' law, which can be expressed as follows:

$$C = \varepsilon_0 \varepsilon_r \frac{A}{d} \tag{1}$$

where ε_0 is the electric constant (8.854 × 10^{-12} F/m), ε_r is the relative static permittivity (1.00054 in air), A is the area of the two plates, and d is the distance between the two plates. However, the calculation formula was modified because interdigital patterns of four line widths, namely 0.25, 0.5, 0.75, and 1.0 mm, were designed and employed as capacitors for investigating the voltage induced by the

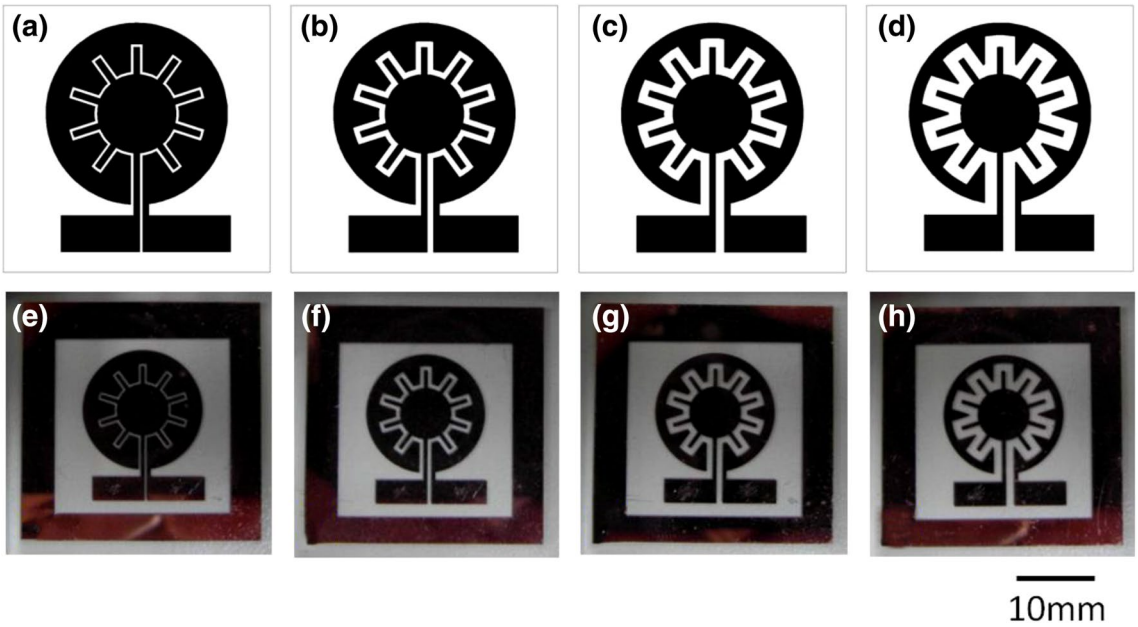

Fig. 3 **a**–**d** Design and **e**–**h** experimental patterns with *line* widths of **a/e** 0.25, **b/f** 0.5, **c/g** 0.75, and **d/h** 1.0 mm

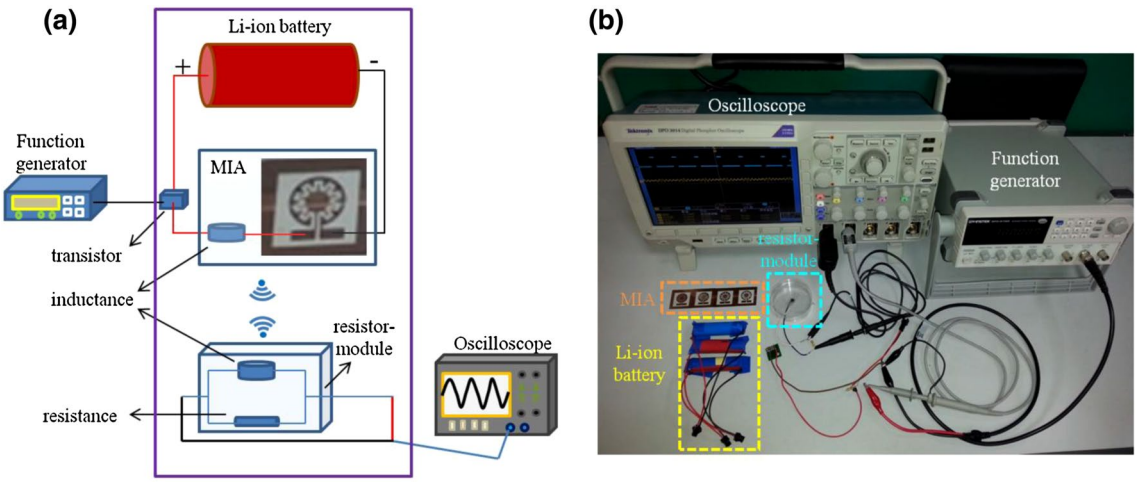

Fig. 4 **a** Schematic and **b** experimental layout of the SOH measuring module

wireless method. As shown in Fig. 3, the dimensions of the design patterns matched the dimensions of the experimental patterns that were ablated by the laser system.

2.3 Design of the measurement module

In the measuring experiment, conversion circuit and the MIA were integrated and build as a micro-device, named SOH meter, to measure the induced voltage and compute the SOH of LIBs. Therein, the MIA consists of the interdigital pattern and a inductance, and the conversion circuit was especially designed and produced and had the advantages of being low cost and having high accuracy and ease of use, as shown in Fig. 4. A function generator was used to control the switch of the transistor, and the MIA emitted a wireless signal when the transistor was turned off. The SOH of an LIB would decrease if the charge–discharge cycle time of the LIB increased, and the emission power of the MIA and induced voltage measured from the oscilloscope (Taktronix DPO3014) would decrease simultaneously. Therefore, the induced voltage from six LIBs with different cycle times were measured in the experiment to evaluate their SOHs, with the relationship between the induced voltage (V_i) and SOH of the LIBs expressed by a three-order polynomial equation as follows:

Table 3 Summary of LIBs with different cycle times

Type	Cycle times
I	0
II	100
III	200
IV	300
V	400
VI	500

$$\mathrm{SOH} = B_3 \times V_i^3 + B_2 \times V_i^2 + B_1 \times V_i + B_0 \quad (2)$$

where B_1, B_2, and B_3 are the coefficients of the first, second, and third order and B_0 is the constant. In the experiment, six LIBs with different cycle times were used to measure the induced voltage and estimate the SOH of LIBs, as summarized in Table 3. In the measuring process, the measured value could be affected by the electromagnetic wave from a cell phone or other electronic equipment; hence, the measurement module should not be employed near an electronic product. Preferably, the measurement should be isolated and conducted in an isolation chamber. In addition, the SOH meter including MIA, conversion circuit, function generator, and other electronic equipments was a prototype system in the manuscript; the above devices would be packaged together as an industry-accepted testing module; and the microcontroller unit will be employed to process the measured data and export a value of SOH of LIB for operators in the future.

3 Experimental results and discussion

3.1 Induced voltage and capacity of the samples processed using laser ablation

When the interdigital patterns were ablated from the continuous films to form the capacitors, the capacitance values were measured by the LCR meter (Aglient U1732 A) at a frequency of 10 kHz, as summarized in Table 4. The results showed that the capacitance value decreased with an increase in the line width of the interdigital pattern. In addition, the induced voltage measured from the microdevice was inversely proportional to the capacitance value and had a maximal response when the pattern with a line width of 0.75 mm was employed, as shown in Fig. 5. The reason that the maximal response occurred with this pattern and line width was that the charge time increased when the capacitor had a high capacitance value and that there was no sufficient time in the experiment for C_1 and C_2 to store enough energy and reach the rated voltage when the operating frequency for switching the transistor was fixed at 500 kHz. Therefore, the voltage charge in the capacitor would decrease if the capacitance value increased, causing the highest induced voltage in C_3 and an induced voltage in C_1 that was lower than that in C_2. By contrast, the energy stored in C_4 was too low to induce enough voltage, causing the measured voltage to decrease. The results showed that the interdigital pattern with a line width of 0.75 mm was most suitable for measuring the SOH of an LIB.

In addition, the value of the induced voltage was affected by the distance between the MIA and resistor modules;

Table 4 Estimated and measured capacitance values of the interdigital patterns

Number	Line width (mm)	Measured capacitance (pF)
C_1	0.25	4
C_2	0.5	3.5
C_3	0.75	3.4
C_4	1.0	2.8

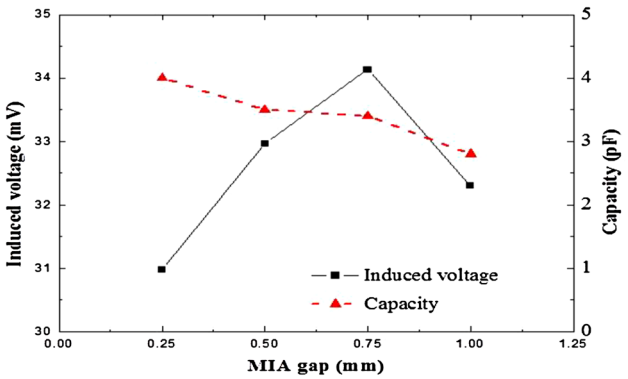

Fig. 5 Induced voltage and capacity of an MIA ablated at different *line* widths

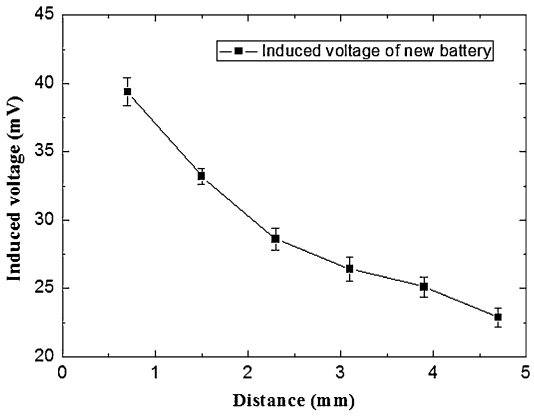

Fig. 6 Induced voltage at different distances of the MIA and resistor modules

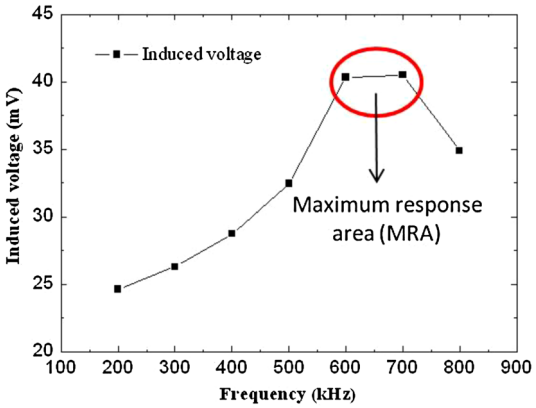

Fig. 7 Induced voltage of an MIA with different operating frequencies

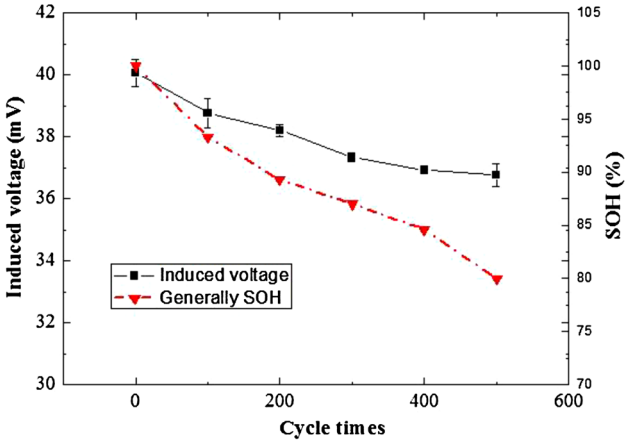

Fig. 8 Induced voltage generally related to the SOH at various cycle times of the LIB

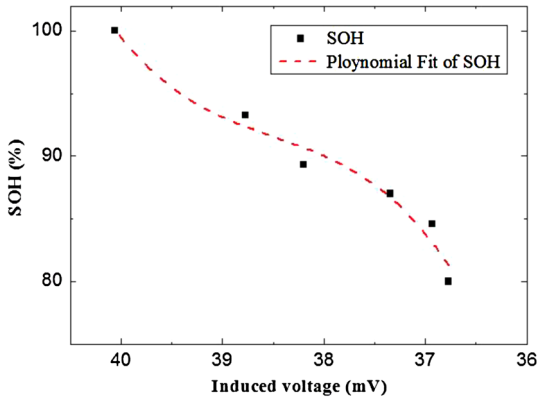

Fig. 9 Relationship between the induced voltage and SOH of an LIB

the value decreased as the distance increased, as shown in Fig. 6. Therefore, the closest distance possible was the most suitable, with the distance in the experiment being set at 0.7 mm.

3.2 Induced voltage of the MIA affected by operating frequency

To determine a suitable operating frequency for enhancing the identification of SOH in LIBs, several frequencies were explored for controlling the switching time of the transistor. The MIA has a back electromotive force (back-EMF) to resist the open circuit created when the transistor is turned off suddenly, and the induced voltage can be measured simultaneously with the back-EMF. The interdigital pattern with a line width of 0.75 mm was employed, and the results showed that the back-EMF and induced voltage increased with an increase in operating frequency because there was enough time to respond to the open circuit, whereas a smaller back-EMF was induced when the operating frequency was low (Fig. 7). The highest induced voltage could be measured at an operating frequency between 600 and 700 kHz and was, therefore, considered to be the maximum response area. However, the transistor could not be turned on when the operating frequency was too high (i.e., higher than 700 kHz) because it would cause the induced voltage to decrease. Therefore, a suitable operating frequency for measuring the SOH of an LIB was determined to be 700 kHz, and a SOH meter was constructed by the MIA and conversion circuit to analyze the SOH of six different LIBs.

3.3 SOH of LIBs

The relationship between the capacity, SOH, and cycle time can be expressed as a third-order polynomial equation. Generally, the SOH of LIBs would decrease to 80 % after 500 charge–discharge cycles. The induced voltage of each LIB was measured three times repeatedly; the three measured LIB values from each cycle time were similar. The average value was then employed to estimate the SOH of the LIBs. The results from measuring the induced voltages of six different LIBs showed that the induced voltage of Type VI decreased to 91.8 % of the value of Type I (Fig. 8) and indicated that the relationship between the induced voltage and cycle time of an LIB was not similar to the relationship between its capacity and cycle time.

SOHs of LIBs of six charge–discharge cycle times from Type I to Type VI were determined to be 100, 93.3, 89.3, 87, 84.6, and 80 % [18], respectively. Coefficient values of 1.06024, −122.42, 4714.71, and −60468.83 were obtained for B_3, B_2, B_1, and B_0, respectively, in Eq. (2) by using the curve-fitting method and the measured induced voltage. Subsequently, the new relationship between the induced voltage (V_i) and SOH was expressed as Eq. (3), as shown

in Fig. 9. From the results, the established curve of SOH and induced voltage was similar to the generally SOH curve related to capacity of LIB. In the future, the SOH of an unknown cycle of an LIB will be computed from the induced voltage measured by the developed SOH meter with a measuring time of only 1 s.

$$\mathrm{SOH} = 1.06025 \times V_i^3 - 122.42 \times V_i^2 + 4714.71 \times V_i - 60468.83 \quad (3)$$

4 Conclusion

In the study, we proposed a micro-device (SOH meter) that includes an interdigital pattern ablated using a UV laser to evaluate the SOH of an LIB and has the advantages of having low production costs, being mask free, and evaluating rapidly. We found that the line width of an interdigital pattern affects the capacity and measured voltage induced from the MIA; the results indicate that an interdigital pattern with a line width of 0.75 mm has a higher response rate than those with other widths do. As shown by the experimental results, a suitable operating frequency for determining the SOH of LIBs is 700 kHz, which can provide improved identification between effective and ineffective batteries. In addition, a new relationship between the induced voltage and SOH of LIBs was established, and the SOH of LIBs can be evaluated from the induced voltage measured from the presented device. Furthermore, the cost time for obtaining the SOH of the LIB by using the presented device was only 1 s, and the results are a suitable reference for manufacturing a portable measurement for the SOH of LIBs and MIA modules.

Acknowledgments The authors thank the Ministry of Science and Technology, Taiwan, for financially supporting this research under contracts "MOST 103-2221-E-492-018" and "MOST 103-2622-E-492-014-CC3."

References

1. A. Jossen, J. Power Sources **154**(2), 530 (2006)
2. M. Broussely, Ph. Biensan, F. Bonhomme, Ph. Blanchard, S. Herreyre, K. Nechev, R.J. Staniewicz, J. Power Sources **146**(1), 90 (2005)
3. S. Piller, M. Perrin, A. Jossen, J. Power Sources **96**(1), 113 (2001)
4. S. Rodrigues, N. Munichandraiah, A.K. Shukla, J. Power Sources **87**(1), 12 (2000)
5. M. Urbain, S. Raël, B. Davat, P. Desprez, in proceedings of IEEE power electronics specialists conference, Orlando, pp 17–21 June (2007)
6. S. Yuan, H. Wu, C. Yin, Energies **6**(1), 444 (2013)
7. G.L. Plette, J. Power Sources **134**(2), 262 (2004)
8. F. Zhang, G.J. Liu, L.J. Fang, H.G. Wang, IEEE Trans. Ind. Electron. **59**(2), 1086 (2012)
9. Y.S. Lee, W.Y. Wang, T.Y. Kuo, IEEE Trans. Ind. Electron. **55**(1), 229 (2008)
10. S.G. Li, S.M. Sharkh, F.C. Walsh, C.N. Zhang, IEEE Trans. Veh. Technol. **60**(8), 3571 (2011)
11. G.L. Plette, J. Power Sources **161**(2), 1369 (2006)
12. J. Groot, *State-of-Health Estimation of Li-ion Batteries: Cycle Life Test Methods* (Göteborg, Sweden, 2012)
13. E. Meissner, G. Richter, J. Power Sources **116**(1), 79 (2003)
14. M. Dubarry, B.Y. Liaw, J. Power Sources **194**(1), 541 (2009)
15. A.N. Bloom, D.P. Jansen, J. Abraham, S.A. Knuth, V.S. Jones, G.L. Battaglia, G.L. Henriksen, J. Power Sources **139**(1), 295 (2005)
16. J.P. Christophersen, S.R. Shaw, J. Power Sources **195**(4), 1225 (2010)
17. R. Spotnitz, J. Power Sources **113**(1), 72 (2003)
18. Website: Battery University, BU-902: How to measure internal resistance. http://batteryuniversity.com/learn/article/how_to_measure_internal_resistance
19. F. Huet, J. Power Sources **70**(1), 59 (1998)
20. P. Singh, S. Kaneria, J. Broadhead, X. Wang, J. Burdick, INTELEC 26th Annual International Telecommunications Energy Conference, Chicago, 524(2004)
21. X. Feng, J. Li, L. Lu, J. Hua, L. Xu, M. Ouyang, J. Power Sources **209**, 30 (2012)
22. S. Tumanski, Induction coils sensors—a review. Meas. Sci. Technol. **18**(3), 31 (2007)
23. N.X. Sun, J.W. Wang, A. Daigle, C. Pettiford, H. Mosallaei, C. Vittoria, Electron. Lett. **43**(8), 434 (2007)
24. G.M. Yang, X. Xing, A. Diagle, M. Liu, O. Obi, J.W. Wang, K. Naishadham, N.X. Sun, IEEE Trans. Magn. **44**(11), 3091 (2008)
25. C.C. Yang, H.Y. Tsai, C.C. Yang, W.T. Hsiao, K.C. Huang, Appl. Phys. A **117**(1), 69 (2014)
26. H.Y. Tsai, C.C. Yang, C.C. Yang, W.T. Hsiao, K.C. Huang, Appl. Phys. A **117**(1), 415 (2014)